4. Liquid-crystal-based tunable terahertz Lyot filter

4.1. Introduction

In the past decade, THz studies ranging from investigations of ultrafast dynamics in materials to medical, environmental sensing and imaging have been actively explored [1-3]. For these and future applications in THz communication and surveillance, quasi-optic components such as filters, phase shifters, attenuators and polarizers are indispensable. Up to now, several designs of THz filters have been reported. These include fixed frequency filters such as two-dimensional metallic hole arrays or photonic crystals (2D-MHA or 2D-MPC) that acts as a band-pass filter or frequency selective surface (FSS) [4,5]. A filter with fixed center frequency of 0.4 THz using a binary grating with rectangular grooves as FSS was also demonstrated [6]. Recently, Wu *et al.* reported a Terahertz plasmonic high pass filter consisting of high-aspect-ratio micron-sized wire arrays [7]. Several type of tunable THz filters have also been demonstrated. These include: a tunable THz attenuator and filter (operating at low temperature) based on a mixed type-I/type-II GaAs/AlAs multiple quantum well structure tuned by optical injection [8]; a metallic photonic crystal filter made tunable over the range of 365-386 GHz by a relative lateral shift of 140 μm between two micro-machined metallic photonic crystal plates [9]. By use of $SrTiO_3$ as a defect material inserted into a periodic structure of alternating layers of quartz and high-permittivity ceramic, Nemec *et al*. [10] was able to tune a single defect mode in the 1-D photonic crystal from 185 GHz at room temperature down to 100 GHz at 100 K by thermal tuning. Voltage controlled wavelength selection at microwave frequencies was

achieved by Yang and Sambles [11] using a structure of metallic slat gratings with the thin grooves between the metallic slats filled with nematic liquid crystal (NLC). Similarly, Tanaka and Sato [12] reported electrically controlled millimeter-wave (up to 94 GHz) transmission properties of stack-layered liquid crystal cells with metal substrates. Recently, we reported control of enhanced THz transmission through 2D-MHA using magnetically controlled birefringence in nematic liquid crystals [13].

The Lyot filter [14], a type of birefringent filters widely employed in the visible and near infrared, is based on interference of polarized light by means of a stack of birefringent elements with their optical axes rotated with respect to each other. Lyot filters can be made tunable using active birefringent retarders such as electro-optic crystals [15] and liquid crystal cells [16]. Recently, we have developed variable phase shifters or retarders with maximum phase shift or retardance exceeding 2π at 1 THz [17,18]. These are based on magnetically controlled birefringence in NLCs, 4'-*n*-pentyl-4-cyanobiphenyl (5CB, Merck) [19,20] or E7 (Merck) [18], both of which exhibit relatively large birefringence (~ 0.2) and small extinction coefficient (<0.05) at THz frequencies. In this chapter, we construct and characterize a room-temperature tunable THz Lyot filter based on magnetically controlled retardation in LC.

4.2. Theory

In generally, polarized light passing through birefringent material changes its state of polarization. The rate of change is proportional to the wave number of the light, inversely proportional to the wavelength, when dispersion effects are neglected. There

are several filters, such as Lyot-Öhman (L-O) filter, and Solč filter, base on this fact have been developed [21].

In the L-O filter, a birefringent plate is placed between the two polarizers, whose polarization axes are parallel to each other and at 45° to the optic axis of the birefringent plate (all perpendicular to the normal to the plates, which shown in Fig. 4.2.1). If the birefringent material is a half-wave plate (λ/2), or an odd multiple thereof, the linearly polarized light entering it will be completely blocked by the second polarizer. This will happen for any wavelength (λ) for which the plate thickness (d) satisfies the condition

$$\lambda = \frac{2d\Delta n}{m}, \quad m = 1,3,5,... \tag{4.2.1}$$

where $\Delta n=|n_e-n_o|$ is the birefringence of the birefringent plate, d is the thickness of the birefringent plate, and m is the odd integers. Indeed, it is readily shown that the transmittance of the sandwich will vary with the wavelength according to

$$T = T_0 \cos^2(\frac{\pi d\Delta n}{\lambda}). \tag{4.2.2}$$

Neglecting dispersion effects, the width, $\delta\lambda$, of the transmission band between half-intensity point can be found from the following consideration. Let m be the number of full-wave cycles represented by d at the peak wavelength λ_0:

$$\frac{\Delta n\, d}{\lambda_0} = m\,. \tag{4.2.3}$$

Thus and desired passband width can be obtained by the appropriate choice of thickness

$$d = \frac{{\lambda_0}^2}{2\delta\lambda\,\Delta n}. \tag{4.2.4}$$

There remains, however, the problem of the additional transmittance peaks appearing, spaced 2 $\delta\lambda$, 4 $\delta\lambda$, etc. Since this spacing is only twice as large as the width of the passband, such a plate, in itself, would not usually be useful as a filter. The basic contribution of Lyot was to eliminate all but the desired transmittance peak over a full octave [14]. He noted that if the above filter is cascaded with another of half the thickness, the nearest transmittance peak will be twice as far away and a transmittance peaks has been halved and their spacing doubled, whereas the peak width has been very slightly reduced. If this is now followed by another such filter whose plate is half as thick as that of its predecessor, and the process is continued until a simple half-wave plate is reached, the first spurious transmittance peak will appear at $\lambda_0/2$. See figure 4.2.2, where (a) shows the transmittance spectrum of a 16 λ plate, (b) that of an 8 λ plate, etc, with (e) showing that of a full-wave plate. Figure 4.2.2 (f) shows the transmittance spectrum of the combination: the product of the transmittance curves (a)-(e), illustrating the peak at λ_0/λ=2. In general, a filter consisting of N birefringent plate of thicknesses d, 2d, 4d ... 2^{N-1}d will have a transmittance of the form

$$T(\lambda) = T_0 \prod_{k-1}^{N} \cos^2 2^{k-1}\Gamma, \tag{4.2.5}$$

where T is the transmittance of the filter when Γ, the retardation of the plate, equals to π, which is given by

$$\Gamma = \frac{2\pi \Delta n\, d}{\lambda}. \qquad (4.2.6)$$

Clearly, the retardation varies the center wavelength, λ_0, according to Eq.4.2.2. There are several methods, which can be used to tune the retardation of the wave plate, such as the effect of the incident angle, temperature effect, etc.

4.3. Experiment

4.3.1. Evaluation and Design

The LC-based Lyot filter has two elements, A and B, which are separated by a linear polarizer (Fig. 4.3.1.1). Each element consists of a fixed retarder (FR) and a tunable retarder (TR). The FR consists of a pair of permanent magnets sandwiching a homogeneously aligned LC cell. Sufficiently large magnetic field is required for quenching the director fluctuation of LC molecules and reducing the scattering in the thick LC cell (inset (a) of Fig.4-2.) The homogeneous cells in FR_A and FR_B supply fixed phase retardations, Γ_A and Γ_B, respectively, for THz waves. The tunable retarders, TR_A and TR_B (inset (b) of Fig. 4-2,) are used to achieve the desired variable phase retardation, $\Delta\Gamma_A$ and $\Delta\Gamma_B$. They are of our previous design [17,18], i.e., a fixed homeotropicly aligned LC cell normal to the z-axis is placed at the center of the magnet rotatable along the x- or y-axis (see Fig. 4.3.3.1). As the magnet rotates to a new position, the LC molecules are reoriented parallel to the new field direction and provides a variable effective index of refraction.

The transmittance, T, of the two-element Lyot filter for normally incident THz wave can be written as [14]

$$T = \cos^2\left(\frac{\Gamma_A + \Delta\Gamma_A}{2}\right) \cdot \cos^2\left(\frac{\Gamma_B + \Delta\Gamma_B}{2}\right). \tag{4.3.1}$$

Because of the birefringence of LC, the THz waves, which pass through each element will be separated into extraordinary and ordinary rays (e-ray and o-ray) with corresponding time delays between the e-ray and o-ray, $\Delta\tau$, and the phase retardation $\Gamma = 2\pi \cdot \Delta\tau \cdot f$ The transmittance of the THz Lyot filter as a function of frequency of the THz waves, f, is then given by

$$T(f) = \cos^2(\pi \cdot \Delta\tau_A \cdot f) \cdot \cos^2(\pi \cdot \Delta\tau_B \cdot f). \tag{4.3.2}$$

The Lyot filter in this work is designed such that $\Delta\tau_B = 2\Delta\tau_A$. Satisfying this condition, $T(f)$ in Eq.4.2.2 becomes

$$T(f) = 4\cos^6(\pi \cdot \Delta\tau_A \cdot f) - 4\cos^4(\pi \cdot \Delta\tau_A \cdot f) + \cos^2(\pi \cdot \Delta\tau_A \cdot f). \tag{4.3.3}$$

The first maximum of $T(f)$ occurs when the condition $\Delta\tau_A \cdot f = 1$ is fulfilled.

The filter can be operated in either the positive mode or negative mode. The terms “positive” and “negative” mean that the corresponding phase retardation provided by the TRs is positive or negative. The frequency tunable range can be extended by operating the filter in both modes. In the positive/negative mode, the rotary axes of the magnets in TR_A and TR_B is parallel to y-/x-axis. The retardations by the TRs, $\Delta\Gamma_A$ and $\Delta\Gamma_B$, are then both positive/negative with respect to the retardation

by the FRs. The angle between the aligned direction of homogeneous cells and the polarization of THz waves is 59°. Discussion about this chosen angle is given later in this article.

4.3.2. Elements preparation

Two kinds of LC cells, the homogeneous and homeotropic cells are used in our filter. Each cell is constructed with two fused silica plates with aluminum spacers and filled with E7 (Daily Polymer Crop., Taiwan). The inner silica surfaces of homogeneous cells are coated with polyimide [22] followed by rubbing while the homeotropic cells are coated with *N*,*N*-dimethyl-*n*-octadecyl-3-aminopropyltrimethoxysilyl chloride (DMOAP) [23], to align the LC molecules parallel and perpendicular to the surface, respectively.

The thicknesses of homogeneous LC layer in the fixed retarders, FR_A and FR_B, are 4.5 and 9.0 mm each. A pair of permanent magnets (sintered Nd-Fe-B) with the magnetic fields (~0.18 Tesla) parallel to the LC cell surfaces is used in order to ensure stable homogeneous alignment [24]. The thickness of LC layers in homeotropic cells for tunable phase retarders, TR_A and TR_B, are 2.0 and 4.0 mm, respectively. An annular permanent magnet (sintered Nd-Fe-B), which is fixed on a rotary stage controlled by computer is employed for providing a rotatable magnetic field in order to re-orientate the molecules of LC. The detail structure of it is same with what we mentioned in Sec. 3.3.

4.3.3. Testing and measurement

The maximum magnetic field at cell position in the rotary permanent magnets (sintered Nd-Fe-B) is 0.427 Tesla. This is much larger than the critical field for alignment of LC molecules (~0.015 T) [24]. It is thus assumed that all LC molecules are parallel to it. The retardation of THz waves transmitted through the homeotropic cells can be tuned by rotating the magnets. The retardation provided by homeotropic cells, TR_A and TR_B will be zero when the LC molecules are parallel to the z-axis and change with the reorientation of the LC molecules by rotating magnets. TR_A and TR_B can be either positive or negative depending on the rotary axes of the magnets that are parallel to the y- or x-axis. The filter was characterized by using a photoconductive-antenna-based THz time-domain spectrometer (THz-TDS) [25]. Briefly, the linear polarized THz pulses generated by femtosecond-laser excited dipole-type antenna fabricated on low-temperature-grown GaAs (LT-GaAs) are collimated by an off-axis paraboloidal mirror, and pass through the filter at normal incidence. The transmitted THz pulses are focused on another dipole-type antenna gated by time-delayed probe pulses and oriented to detect THz waves polarized parallel to both of the incident THz wave polarization and the polarizer between the two elements. The measurements are done at room temperature (~25ºC).

The filter is tuned by rotating the magnets in TR_A and TR_B synchronously such that the condition $\Delta\tau_B=2\Delta\tau_A$ remains satisfied. To ensure fulfilling of this criterion, the dependence of $\Delta\tau_B$ and $\Delta\tau_A$ on rotation of the magnets have been calibrated independently shown in Fig. 4.2.3.1. The open circles and circles are the measured phase retardation and the curves are the fitting results. The left and right axes are with

different unit of ps and degree, respectively. The desired $\Delta\tau_B$ and $\Delta\tau_A$ can thus be obtained by rotating the magnets by the appropriate angle according to the calibration.

4.4. Results

An example of the transmitted THz spectrum through the filter with the $\Delta\tau_A$=2.2 ps (the magnet is not rotated), normalized to the maximum of transmittance, is shown in Fig. 4.4.1. The transmitted peak frequency and the band width of the filter are 0.465 THz and ~0.10 THz, respectively. The corresponding THz temporal profile with total retardation, $\Delta\Gamma$=0 is shown in the inset of Fig. 2. Note that there are four peaks with peak separations equal to $\Delta\tau_A$. This can be understood as follows: The THz wave is separated into o-ray and e-ray after passing the first element and these two waves are further separated into o-o-ray, e-o-ray, o-e-ray and e-e-ray, respectively, again after passing the second element. Note that the above arguments are only approximately or qualitatively correct. If the time delay is small, the separation can not be observed this way. The transmission spectrum can be considered as manifestation of the interference among the four peaks of the THz signal in the time domain. The theoretical curve according to Eq.4.3.2 is shown as the solid curve, which is in good agreement with the experimental data. The birefringence of E7 estimated from the $\Delta\tau_A$ and the thickness of the LC layer is 0.155 in the sub-THz frequency range. This is somewhat smaller than what we reported previously (0.170) [18]. It is also lower than that in the visible but in accord with reported dielectric anisotropy in the microwave and millimeter wave range [11]. Conceivably, the effect of thermal fluctuations of molecular orientations in an LC layer as thick as 9 mm could significantly reduce the effective

birefringence of the LC. Note that we used cells much thicker than that in the 1.5 mm cells used in our previous work.

The temporal profiles of transmitted THz waves with different $\Delta\tau_A$ are shown in Fig. 4.4.2. The temporal THz profile is split from one peak into four peaks after passing through the two elements of the filter. The equal time difference, $\Delta\tau_A$, between each peak can be observed from measured data. The transmitted frequency spectrum comes from the interference of these four parts of the THz signal and can be obtained by applying fast Fourier Transform (FFT) to the temporal signals. The peak transmitted frequencies of the filter versus $\Delta\tau_A$ are shown in Fig. 4.4.3. The solid line is the theoretical curve according to $\Delta\tau_A \cdot f = 1$. The peak transmission frequency of the filter decreases with the increasing $\Delta\tau_A$. The tuning range of the filter is from 0.388 to 0.564 THz or a fractional tuning range of ~ 40%.

4.5. Discussion

4.5.1. Azimuthal angle issue

Consider the case of a general Lyot filter consisting of a phase retarder between a pair of polarizers, of which the polarization directions are parallel to each other. The angle, ϕ, between the slow axis of the retarder and the polarization direction of the polarizers, will affect the ratio of electric field amplitudes of e-ray and o-ray without changing the retardation. As the peak transmitted frequency of the Lyot filter depends only on the retardation (See Eq.4.3.1), the spectral distribution of electromagnetic wave transmitted trough the Lyot filter is not affected by the angle ϕ. On the other hand, the transmitted waves can be viewed as the interference of e-ray and o-ray

propagating through the elements. Complete interference will only occur when the field amplitudes of the e-ray and o-ray are equal. In general, this condition can be achieved when ϕ=45° for a retarder, which does not absorb the incident electromagnetic waves. The absorption of E7 (κ<0.05) in THz range is small [18]. The major losses in this work are scattering loss, which is due to the thermal fluctuation of LC molecular orientations [26]. Further, the loss of ordinary ray is larger than that of the extraordinary ray in E7.

We have measured the peak amplitude of the transmitted THz electric fields for o-ray and e-ray as a function of ϕ. The measured profiles of temporal THz signals are shown in Fig. 4.5.1.1. The peak amplitudes versus ϕ are shown as open circles (o-ray) and triangles (e-ray) in Fig. 5, respectively. Recall that the electric field amplitudes of o-ray and e-ray are functions of ϕ:

$$E_o(\phi) = C \cdot \sin^2(\phi) \qquad (4.5.1.1)$$

and

$$E_e(\phi) = D \cdot \cos^2(\phi), \qquad (4.5.1.2)$$

where C and D are constants and can be determined from measured transmission data when ϕ is 0° and 90°, respectively. The solid curves in Fig. 5 are plotted according to Eqs.4.5.1.1 and4.5.1.2. Both the theoretical predictions and experimental data show that the ratio of $E_o(\phi)$ and $E_e(\phi)$ is indeed equal to 1 when ϕ=59°.

4.5.2. Improvement

The insertion loss of the device is around 8 dB. It is attributed mainly to the scattering of the LC molecules of the thick cells (4.5 and 9 mm) used as fixed retarders. This can be improved by using a multilayer structure consisting of several thin LC cells or employing LC with birefringence as high as 0.37 (versus ~ 0.2 for E7) at microwave frequencies reported for a special mixture from Merck [27]. With the use of such LC, we can reduce the thickness of FRs to 4 and 2 mm. On the other hand, the function of the fixed retarders is providing a fixed phase retardation, which can be also achieved by using other birefringent crystals.

4.6. Summary

In summary, we have demonstrated for the first time a tunable room-temperature THz tunable Lyot filter. The key elements are fixed and variable liquid crystal phase retarders. The central passband frequency of the filter can be continuously tuned from 0.388 THz to 0.564 THz (a fractional tuning range of 40%) using magnetically controlled birefringence in nematic liquid crystals. The insertion loss of ~8 dB is attributed to scattering of the LC molecules in the thick LC cells. The bandwidth of the present device is 0.1 THz . Still narrower bandwidth is possible by adding more elements. This filter can be operated at room temperature. The experimental results are in agreement with theoretical predictions. Extension of the LC-based Lyot filter to the higher THz frequency range (10~30 THz) or mid-infrared is straight forward, with additional benefits of still larger tunable range because of the shorter wavelength.

Bibliography

1. D. Mittleman, ed., *Sensing with Terahertz Radiation* (Springer-Verlag, Berlin, 2003).
2. P. H. Siegel, *IEEE Trans. Microwave Theory Tech*. **50**, 910 (2002).
3. B. Ferguson and X.-C. Zhang, *Nature Materials*, **1**, 26 (2002).
4. T. K. Wu, *Frequency Selective Surface and Grid Array* (Wiley, New York, 1995).
5. C. Winnewisser, F. T. Lewen, M.Schall, M. Walther, and H. Helm, *IEEE Trans. Microwave Theory Tech*. **48**, 744 (2000).
6. S. Biber, A. Hofmann, R. Schulz, M. Collischon, J. Weinzierl, and L. P. Schmidt, *IEEE Trans. Microwave Theory Tech.*, **52**, 2183 (2004).
7. D.M. Wu, N. Fang, C. Sun, X. Zhang, W.J. Padilla, D.N. Basov, D.R. Smith and S. Schultz, *Appl. Phys. Lett.*, **83**, 201 (2003).
8. I. H. Libon, S. Baumgärtner, M. Hempel, N. E. Hecker, J. Feldmann, M. Koch, and P. Dawson, *Appl. Phys. Lett.* **76**, 2821 (2000).
9. T. D. Drysdale, I. S. Gregory, C. Baker, E. H. Linfield, W. R. Tribe, D. R. S. Cumming, *Appl. Phys. Lett*. **85**, 5173 (2004).
10. H. Nemec, P. Kuzel, L. Duvillaret, A. Pashkin, M. Dressel, M. T. Sebastian, *Opt. Lett.*, **30**, 549 (2005).
11. F. Yang and J. R. Sambles, *Appl. Phys. Lett*., **79**, 3717 (2001).
12. M Tanaka, S Sato, *J. J. Appl. Phys*., **40,** 4131 (2001).
13. C.-L. Pan, C.-F. Hsieh, and R.-P. Pan , M. Tanaka, F. Miyamaru, M. Tani, and M. Hangyo, *Opt. Express*, **13**, 3921, 2005.
14. B. Lyot, *Ann. Astrophys.*, **7**, 31 (1944).

15. B. H. Billings, *J. Opt. Soc. Am.,* **37**, 738 (1947).
16. W. I. Kaye, U.S. Patent No. 4,394,069 (19 July 1983).
17. C.-Y Chen, T.-R Tsai, C.-L. Pan, and R.-P. Pan, *Appl. Phys. Lett*. **83**, 4497 (2003).
18. C.-Y. Chen, C.-F. Hsieh, Y.-F. Lin, R.-P. Pan, and C.-L. Pan, *Opt. Express*, **12**, 2625 (2004).
19. T.-R. Tsai, C.-Y. Chen, C.-L. Pan, R.-P. Pan, and X.-C. Zhang, *Appl. Opt*. **42**, 2372 (2003).
20. R.-P. Pan, T.-R. Tsai, C.-Y. Chen, C.-H. Wang, and C.-L. Pan, *Mol. Cryst. Liq. Cryst.*, **409**, 137(2003).
21. Leiv Leo, *Appl. Optics*, 1960.
22. M. Nakamura, *J. Appl. Phys.*, **52**, 4561(1981).
23. F. J. Kahn, *Appl. Phys. Lett*., **22**, 386 (1973).
24. P. G. de Gennes and J. Prost, *The Physics of Liquid Crystals*, **2nd ed.** (Oxford, New York, 1983).
25. S. Nashima, O. Morikawa, K. Takata, and M. Hangyo, *J. Appl. Phys*. **90**, 837 (2001).
26. W.T. Coffey and Y.P. Kalmykov, *Liq. Crys.*, **14**, 1227 (1993).
27. C. Weil, S. Muller, R. Scheele, P. Best, g. Lussem, R. Jakoby, *Electron Lett*., **39**, 1732 (2003).

Figure

Figure 4.2.1

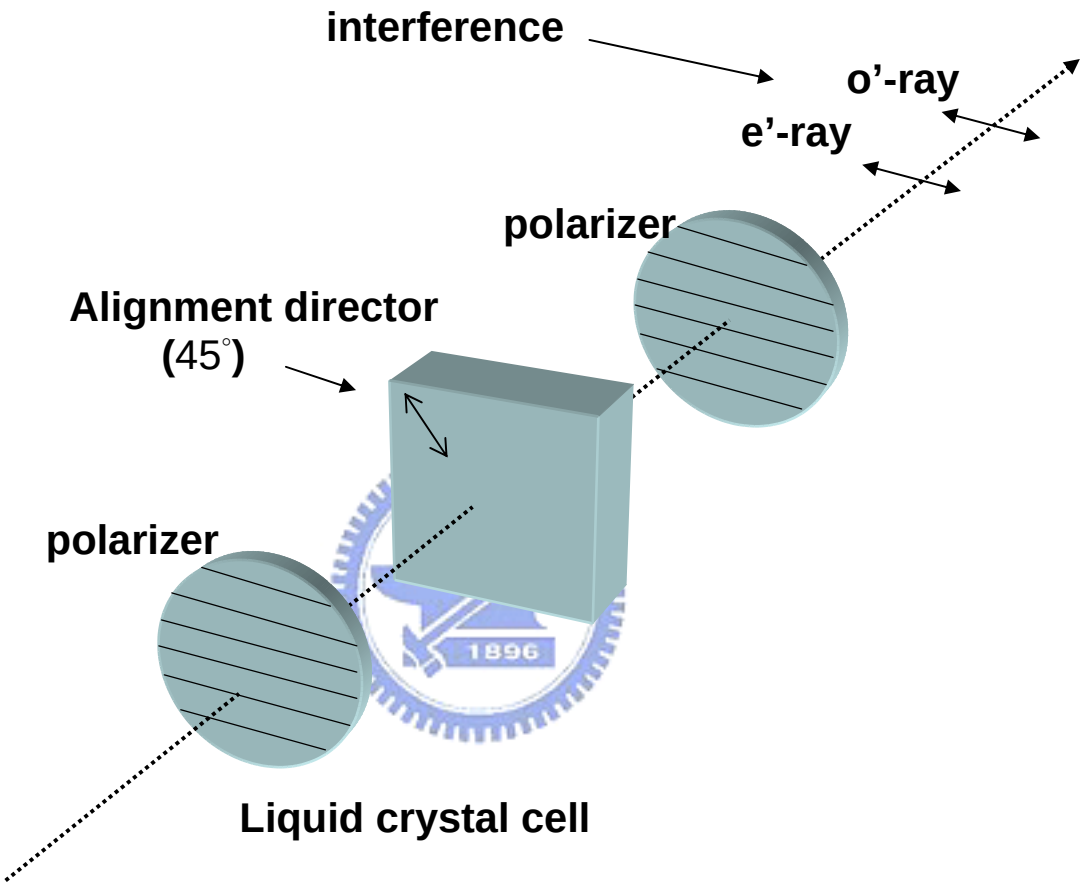

Figure 4.2.1 The general structure of Lyot filter: a birefringence plate placed between a pair of parallel polarizers, whose polarization axes are parallel to each other and at 45º to the optic axis of the birefringent plate.

Figure 4.2.2

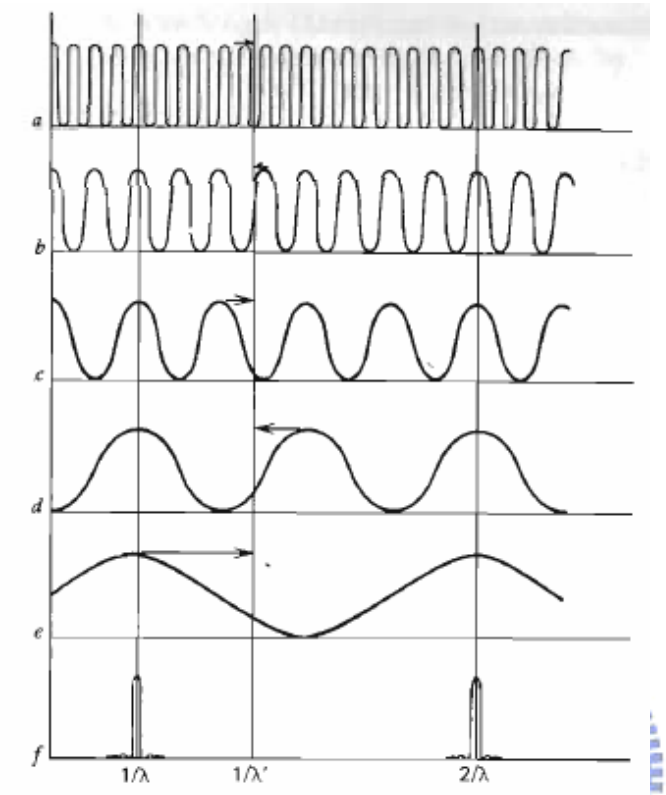

Figure 4.2.2 (a) shows the transmittance spectrum of a 16 λ plate, (b) that of an 8 λ plate, etc, with (e) showing that of a full-wave plate. Figure 4.2.2 (f) shows the transmittance spectrum of the combination: the product of the transmittance curves (a)-(e), illustrating the peak at $\lambda_0/\lambda=2$ [21].

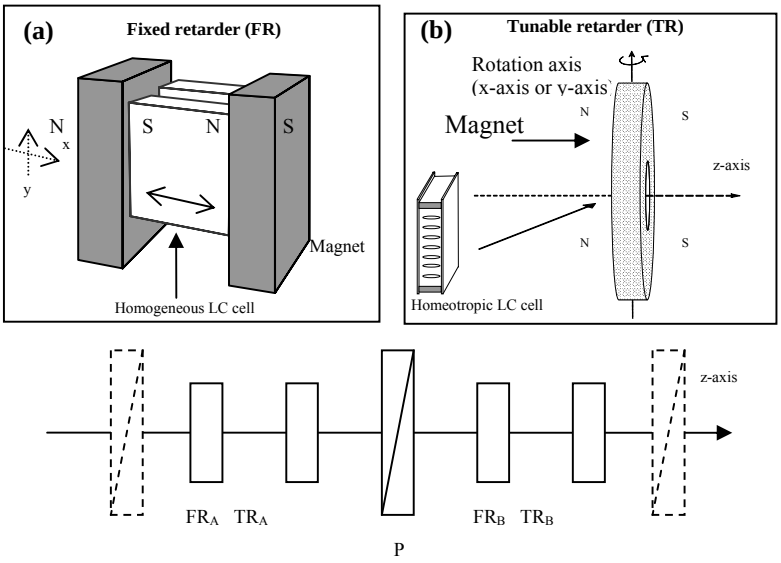

Figure 4.3.1.1 The schematic diagram of the LC-based Lyöt filter: The fixed retarder (inset (a)) consists of a homogeneous LC cell, which sandwiched by a pair of platy magnets. The tunable retarder (inset (b)) consists of a homeotropic LC cell and a magnet.

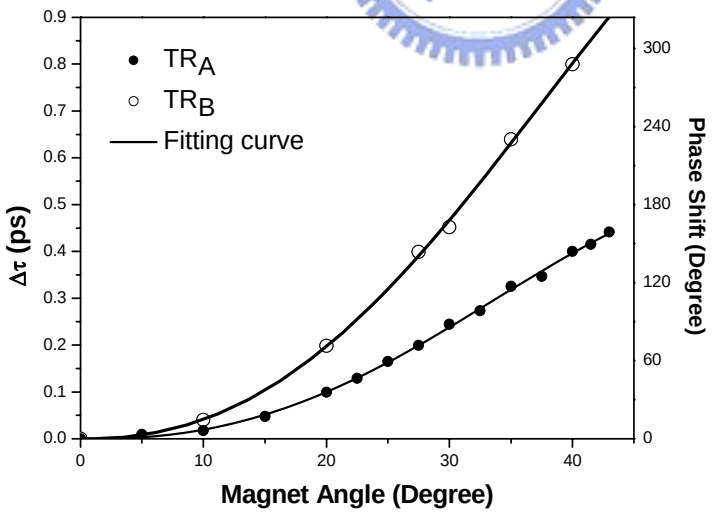

Figure 4.3.3.1 The calibration of TRA and TRB with the Δτ versus magnet angle. The open circles and circles are the measured data and the curves are the fitting results.

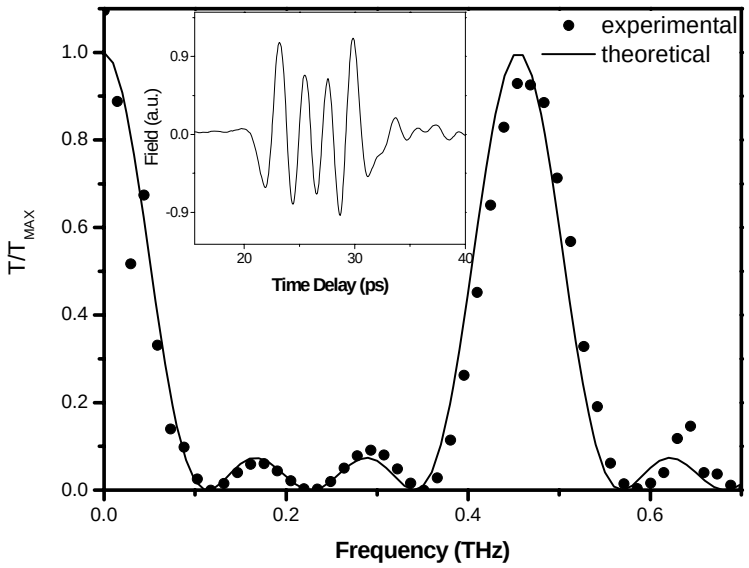

Figure 4.4.1 The transmitted spectrum of the THz waves by applying FFT on the measured temporal THz signal. The measured THz signal is shown in the inset. The circles are the measured results and the curve is theoretical prediction from Eq. (4.3.3).

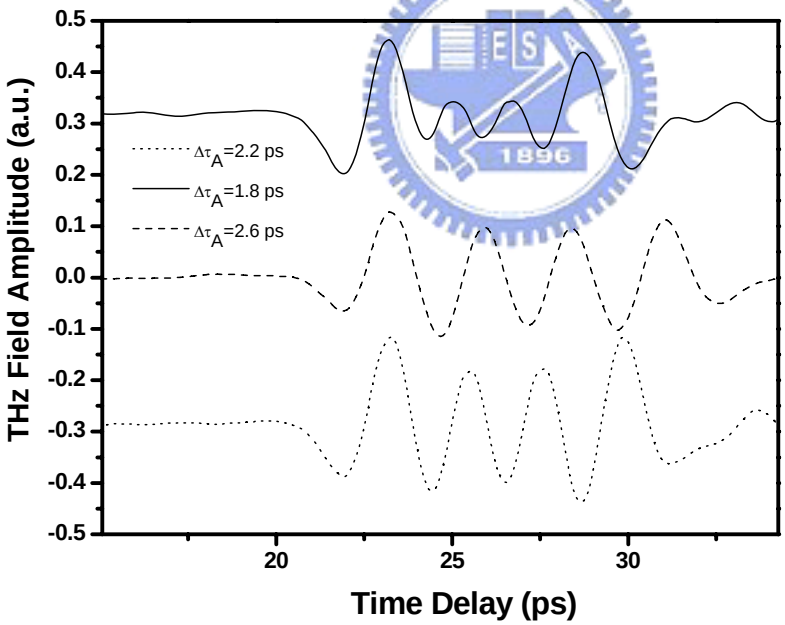

Figure 4.3.2 The measured temporal THz signals with $\Delta\tau_A$=1.8, 2.2 and 2.6 ps.

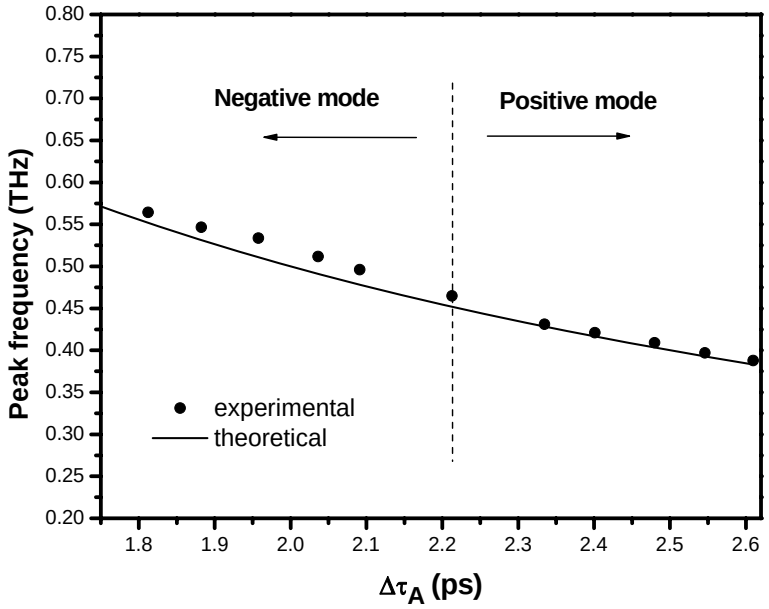

Figure 4.4.3 The peak transmitted frequencies of filter versus $\Delta\tau_A$. The circles are the measured results and the curve is theoretical prediction from Eq. (4.3.3).

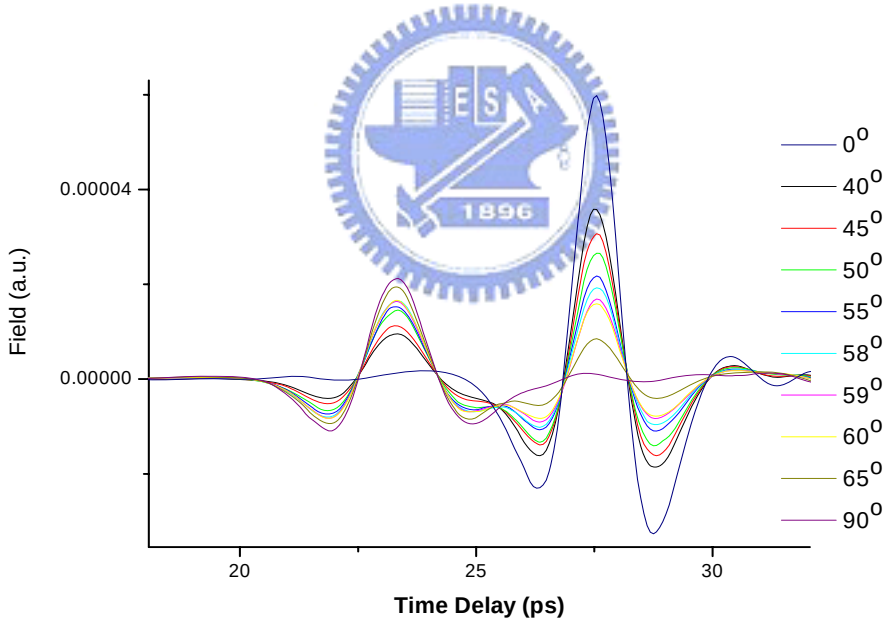

Figure 4.4.1.1 The profiles of the temporal THz signals versus the azimuthal angle.

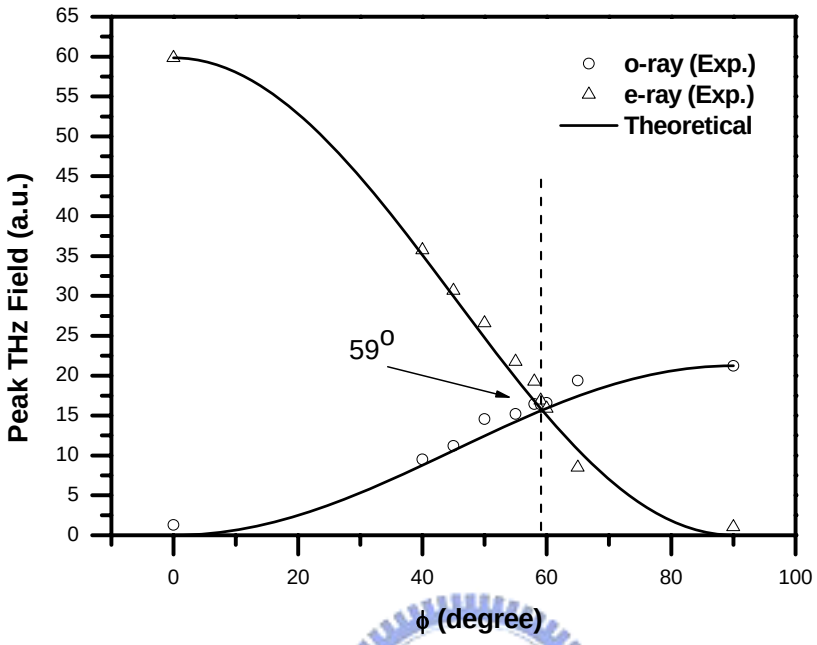

Figure 4.4.1.2 The THz electric fields of e-ray and o-ray versus ϕ. The open circles and open triangles are the measured results from o-ray and e-ray, respectively. The curves are the theoretical predictions from Eq. (4.5.1.1) and Eq. (4.5.1.2) and measured data.